

## Direct observation of bond formation in solution with femtosecond X-ray scattering

The making and breaking of atomic bonds in molecules are essential processes in chemical reactions. The ultrafast bond-breaking processes in various molecular systems have been intensively investigated using time-resolved techniques for several decades [1]. In contrast, the ultrafast bond-making process, especially in solution, has been generally acknowledged that it is more difficult to be investigated due to its bimolecular nature. In a bond-making process, two reactant parties should meet first by slow diffusion through solvent, as a result, it is difficult to synchronize the bond formations in all reactant pairs with laser excitation. In this regard, a gold trimer complex,  $[\text{Au}(\text{CN})_2^-]_3$ , offers a good model system for investigating the ultrafast dynamics of the bond-making process in solution. In the ground state of the complex, gold atoms are weakly bound to each other by a non-covalent interatomic interaction known as aurophilicity [2]. Formation of covalent bonds between adjacent Au atoms can be triggered by laser excitation without the limitation of slow diffusion [3].

We performed the X-ray solution scattering experiments at BL3 beamline of SACLA and NW14A beamline of KEK to capture the moment of the bond formation in the gold trimer complex as well as revealing the detailed structural dynamics. Experimental scheme for the experiment is illustrated in Fig. 1. We obtained

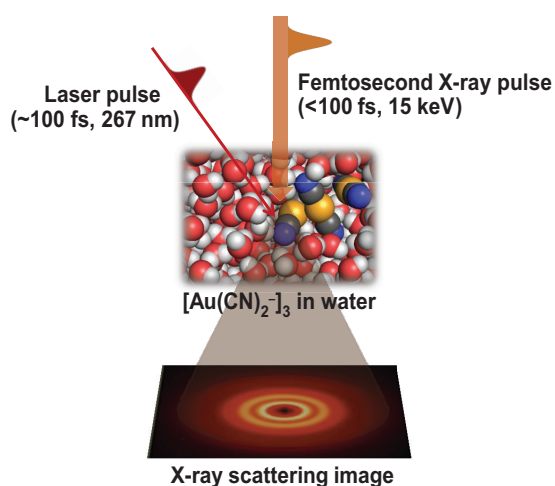


Fig. 1. Schematic of femtosecond X-ray solution scattering experiment. In the gold trimer sample in an aqueous solution, bond formations between adjacent gold atoms are triggered by a laser excitation at 267-nm wavelength. Then, the structural evolution is identified by scattering information arising from a subsequent femtosecond X-ray pulse. Scattered light is detected by a fast two-dimensional charge-coupled device (CCD) detector.

experimental difference scattering curves,  $\Delta S(q)$ , measured at various time delays from  $-800$  fs to  $300$  ns by subtracting scattering curves measured before the laser excitation. The time-resolved difference scattering curves are shown in Fig. 2(a). Then, time-resolved radial distribution functions (RDFs),  $r^2S(r)$ , shown in Fig. 2(b) were calculated by performing Fourier sine transformation on  $q\Delta S(q)$ . Considering that the contributions from C and N atoms on total scattering intensities are essentially negligible, the RDFs actually represent the interatomic distances among the Au atoms of  $[\text{Au}(\text{CN})_2^-]_3$  in real space. The distances of the  $\text{Au}_1\text{-Au}_2$  pair ( $R_{12}$ ) and the  $\text{Au}_2\text{-Au}_3$  pair ( $R_{23}$ ) are encoded by the position of a  $p_1$  peak, and the  $\text{Au}_1\text{-Au}_3$  ( $R_{13}$ ) distance is represented by a  $p_2$  peak. Considering positions of the two peaks at a time delay of  $-800$  fs ( $\sim 3.6$  Å and  $\sim 5.56$  Å for  $p_1$  and  $p_2$ , respectively), Au atoms in the ground state,  $S_0$ , are weakly bound to each other compared to a typical Au-Au covalent bond ( $\sim 2.7$  Å), and the  $S_0$  state has a bent structure. Compared to the  $S_0$  state, at a time delay of  $200$  fs,  $R_{12}$  and  $R_{23}$  both decrease

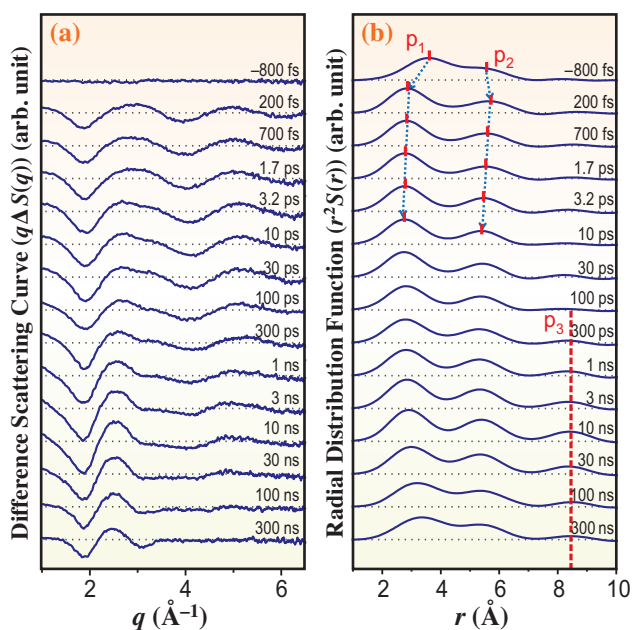


Fig. 2. (a) Experimental difference scattering curves,  $q\Delta S(q)$ , measured at time delays from  $-800$  fs to  $300$  ns. (b) RDFs,  $r^2S(r)$ , obtained by the Fourier sine transformation of  $q\Delta S(q)$ . The blue dashed arrows represent the evolution of the positions of the  $p_1$  and  $p_2$  peaks. The red dashed line indicates the position of the  $p_3$  peak.

significantly ( $\sim 2.8$  Å), indicating the formation of an Au-Au covalent bond at this moment. In contrast,  $R_{13}$  increases slightly ( $\sim 5.63$  Å), which is similar to the sum of  $R_{12}$  and  $R_{23}$ , indicating that a conformational transition occurs from the bent to the linear geometry.

By performing subsequent kinetic analysis on the time-resolved RDFs, we identified four structurally distinct states, the ground ( $S_0$ ) state, an excited ( $S_1$ ) state, a triplet ( $T_1$ ) state and a tetramer, and obtained species-associated RDFs (Fig. 3(a)) as well as their kinetics (Fig. 3(b)). The detailed three-dimensional structures of the four states were reconstructed through a structural fitting analysis with sub-angstrom spatial resolution. The resulting structural parameters ( $R_{12}$ ,  $R_{23}$  and  $R_{13}$ ) are presented in Fig. 3(a). The  $S_0$  state has weakly bounded Au atoms in a bent

geometry, as can be inferred from Fig. 2(b), and it is converted to the  $S_1$  state within our experimental time resolution,  $\sim 500$  fs. In the  $S_1$  state, Au atoms are bound to each other by covalent bonds and aligned in a linear geometry. The time scale of the bent-to-linear structural transition determined from our experiment is in good agreement with that predicted from a previous theoretical study [4]. The  $S_1$  state is further converted to the  $T_1$  state with a time constant of 1.6 ps, accompanying a contraction of the two Au-Au bonds induced by the formation of stronger Au-Au bonds. The  $T_1$  state retains a linear structure similar to that in the  $S_1$  state. Finally, we observed the formation of tetramer species at  $\sim 3$  ns, which can be also recognized due to the appearance of the  $p_3$  peak shown in Fig. 2(b) corresponding to the  $Au_1$ - $Au_4$  pair distance ( $R_{14}$ ). The tetramer ultimately recovers to the  $S_0$  state with a time constant of 100 ns.

In summary, we have demonstrated the capability of XFEL-based femtosecond TRXSS by scrutinizing the reaction mechanism of the formation of covalent Au-Au bonds in the  $[Au(CN)_2]_3$  complex [5]. Femtosecond TRXSS can be used as a fundamental tool to study the structural dynamics of chemical and biological systems in solution by visualizing the structural evolution with high spatial and temporal resolutions.

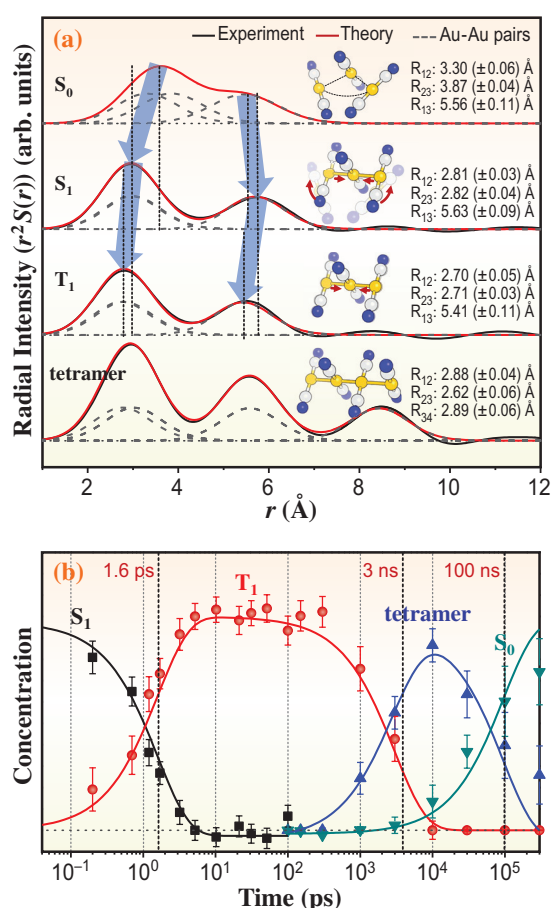


Fig. 3. (a) Species-associated RDFs for the four states obtained by the singular value decomposition and principal-component analyses (black) and their fits (red) obtained by structural fitting analyses. For each state, the structural parameters obtained from structural fittings are shown with their standard errors determined from 50 independent measurements. (b) Concentration changes of the four states. The notations for the four states and the time constants of their transitions are shown.

Jong Goo Kim<sup>a,b</sup>, Hyotcherl Ihee<sup>a,b,\*</sup> and Shin-ichi Adachi<sup>c,d</sup>

<sup>a</sup> Center for Nanomaterials and Chemical Reactions,

Institute for Basic Science, South Korea

<sup>b</sup> Dept. of Chemistry, KAIST, South Korea

<sup>c</sup> Institute of Materials Structure Science, KEK

<sup>d</sup> Dept. of Materials Structure Science,  
The Graduate University for Advanced Studies

\*E-mail: hyotcherl.ihee@kaist.ac.kr

## References

- [1] H. Ihee *et al.*: Science **309** (2005) 1223.
- [2] S.G. Wang *et al.*: J. Am. Chem. Soc. **126** (2004) 1266.
- [3] M.A. Rawashdeh-Omary *et al.*: J. Am. Chem. Soc. **123** (2001) 11237.
- [4] G. Cui *et al.*: Angew. Chem. Int. Ed. **52** (2013) 10281.
- [5] K.H. Kim, J.G. Kim, S. Nozawa, T. Sato, K.Y. Oang, T.W. Kim, H. Ki, J. Jo, S. Park, C. Song, T. Sato, K. Ogawa, T. Togashi, K. Tono, M. Yabashi, T. Ishikawa, J. Kim, R. Ryoo, J. Kim, H. Ihee and S. Adachi: Nature **518** (2015) 385.